T2R2 東京科学大学 リサーチリポジトリ
Science Tokyo Research Repository

論文 / 著書情報
Article / Book Information

Title	Mechanical Behavior of Widening Prestressed Concrete Deck Slabs under Concentrated Load
Authors	Fakhruddin, Takuro Nakamura, Yuji Sato, Masahiko Yamada, JUNICHIRO NIWA
Citation	Journal of Advanced Concrete Technology, Vol. 15, No. 2, p. 38-54
Pub. date	2017, 2

Powered by T2R2 (Science Tokyo Research Repository)

Journal of Advanced Concrete Technology
Materials, Structures and Environment

Mechanical Behavior of Widening Prestressed Concrete Deck Slabs under Concentrated Load

Fakhruddin, Takuro Nakamura, Yuji Sato, Masahiko Yamada, Junichiro Niwa

Journal of Advanced Concrete Technology, volume 15 (2017), pp. 38-54

Related Papers Click to Download full PDF!

Shear Strength of Fiber Reinforced Reactive Powder Concrete Prestressed Girders without Stirrups
Yen Lei Voo, Stephen J. Foster, R. Ian Gilbert
Journal of Advanced Concrete Technology, volume 4 (2006), pp. 123-132

Evaluation on Shear Crack Width in I-shaped Prestressed Reinforced Concrete Beams
Sudhira De Silva, Hiroshi Mutsuyoshi, Eakarat Witchukreangkrai
Journal of Advanced Concrete Technology, volume 6 (2008), pp. 443-458

Click to Submit your Papers

Japan Concrete Institute http://www.j-act.org

Scientific paper

Mechanical Behavior of Widening Prestressed Concrete Deck Slabs under Concentrated Load

Fakhruddin[1*], Takuro Nakamura[2], Yuji Sato[3], Masahiko Yamada[3] and Junichiro Niwa[4]

Received 28 August 2016, accepted 22 January 2017 doi:10.3151/jact.15.38

Abstract

In a technique for widening prestressed concrete (PC) deck slabs, the connection between the old and new deck slabs is crossed by reinforcement and subjected to external prestressing force. A total of six PC deck slabs under a concentrated load were tested to evaluate the effect of the initial prestressing level, concrete strength of the new deck slab, and surface roughness of the interface. A three-dimensional FEM analysis was also conducted to complement the experimental results. The results showed that all PC deck slabs failed in a brittle manner when shear cracks developed at the interface between the old and new deck slabs. Thus, the effective area of the interface for the PC deck slabs under a concentrated load is proposed in this study. Furthermore, by using the value of the effective area instead of the total area of the interface, it has been confirmed that predicted shear capacities obtained from JSCE Specification, AASHTO, and *fib* Model Code 2010 provided a good lower limit for the experimental ultimate capacities.

1. Introduction

Some highway bridges have become functionally obsolete due to inadequate width before they become structurally deficient. Due to the long construction period, high cost, and traffic interruption during demolition, highway widening has become common because it is more economical than the complete replacement.

In the conventional prestressed concrete (PC) box girder bridge widening technique as shown in **Fig. 1(a)**, the existing prestressing tendons need to be connected to the new deck slab. Consequently, some concrete parts should be demolished (around 1000 mm) to expose the tendons from the old deck slabs. The cast-in-place concrete slabs and beams are also required for the widening structure. Therefore, some problems still exist, such as the need to connect the prestressing tendons, the massive wet work of the cast-in-place concrete, and high volumes of formwork, which entail great time and cost.

The new PC box girder bridge widening technique developed by Masui *et al*. (2016) can potentially reduce the cost and improve the speed of construction of bridges. The key components of this widening technique are illustrated in **Fig. 1(b)** and the construction sequences are explained as follows: First, the precast ribs are attached individually to the old bridge by introducing the first prestressing force through the lower PC cables. The longitudinal distance between two precast ribs is 3000 mm. The precast PC panels are then placed between the adjacent PC ribs. After that, some concrete parts in the old deck slabs are demolished (around 200 mm) to expose the embedded rebars. The embedded rebars are then connected with the new rebars by using enclosed welding. Finally, concrete is placed on-site, resulting in a 200-mm-thick layer over the precast PC panels. Shear stress transfer between the old and new deck slabs is achieved by introducing the prestressing force through the upper PC cables. Consequently, the interface between the old and new deck slabs will be subjected to the compression force and the negative bending moment simultaneously. The compression force produces the compressive stress over the entire area of the interface. Meanwhile, the negative bending moment produces the tensile stress and the compressive stress at the top and bottom fiber of the interface, respectively. Since the compressive stress at the top fiber of the interface was predominant than the tensile stress, the entire area of the interface will be compressed. Therefore, the effect of the bending moment can be neglected in the real structure.

Although the new widening technique has considerable merit, the mechanical behavior of widening PC deck slab is still difficult to predict. The two-way interaction is complex and simplified analysis technique does not consider the shear failure mode with the existence of the interface between the old and new deck slabs. The most common failure mode is the punching shear. Many researchers (Higashiyama and Matsui 1998; Hamada *et al*. 2008; Muttoni *et al*. 2012; Clement *et al*. 2013) have proposed the equation to predict the punching shear capacities. Significant work was also performed by Mander *et al*. (2011) to investigate the full-depth precast concrete bridge deck cantilevers,

[1]Ph.D. Candidate, Department of Civil Engineering, Tokyo Institute of Technology, Japan. *Corresponding author, E-mail: *fakhruddin.m.aa@m.titech.ac.jp ;* fakhrud.civil05@gmail.com
[2]Assistant Professor, Department of Civil and Environmental Eng., Tokyo Institute of Technology, Japan.
[3]Technical Section, Fuji P.S. Corporation, Japan.
[4]Professor, Department of Civil and Environmental Eng., Tokyo Institute of Technology, Japan.

which failed in a flexural and shear mixed failure at the panel-to-panel connection. The failure capacity is calculated by using the modified yield line theory. Another potential failure mode is the shear failure of the interface between the old and new slabs. Unfortunately, there are no predictive equations that consider such a failure mode for the PC deck slabs.

In this regard, this study aims to investigate the behavior of the PC deck slab with the existence of the interface between the old and new deck slabs. The experimental parameters were the initial prestressing level, concrete strength of the new deck slab, and surface roughness of the interface. Moreover, a nonlinear 3D FEM analysis was also conducted to complement and verify the experimental results. Finally, the experimental results were compared with the predicted shear capacities using JSCE Specification (2007), AASHTO (2007), and *fib* Model Code 2010 (2013).

2. Experimental and analytical program

2.1 Experimental program

a) Concept design of specimens

This study was designed to simulate the behavior of deck slabs between two precast ribs, having longitudinal distance of 3000 mm as shown in **Figs. 2a** and **b**. Two im-

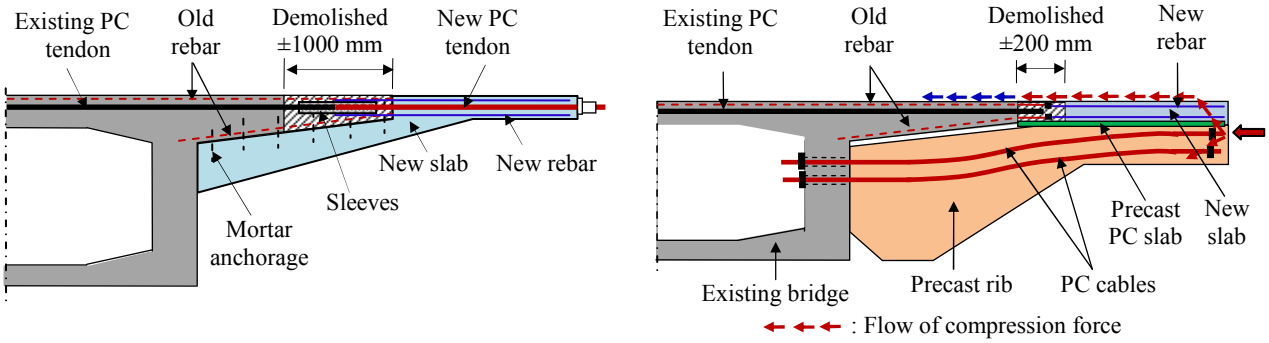

(a) Conventional PC box girder bridge widening technique

(b) Proposed PC box girder bridge widening technique

Fig. 1 Comparison between the common and proposed PC box girder bridge widening technique.

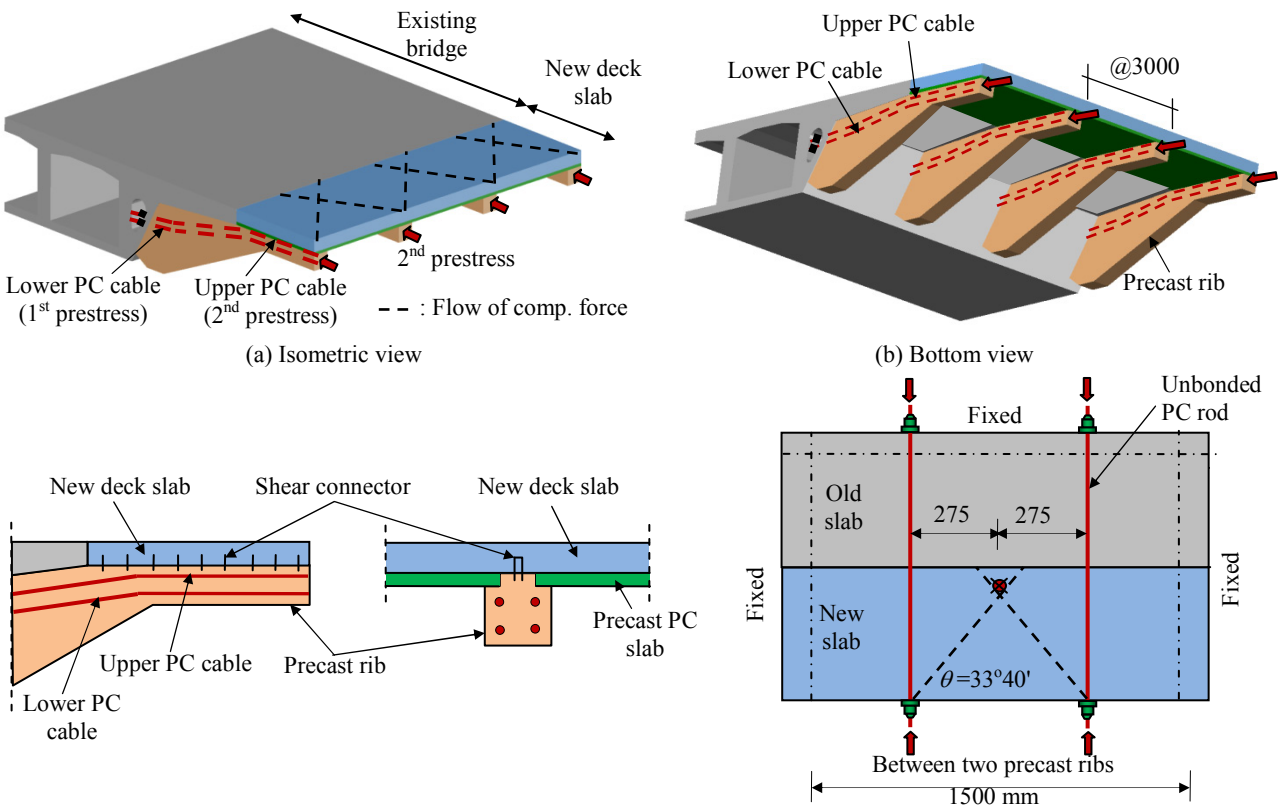

(a) Isometric view

(b) Bottom view

(c) Location of shear connectors

(d) Experimental model (half scale)

Fig. 2 Concept design of specimen.

Table 1 Details of specimens and material properties.

Series	Specimen	σ_i (MPa)	f_c' (MPa)		f_t (MPa)		Surface roughness
			Old slab	New slab	Old slab	New slab	
I, II and III	SL-P1.0	1.0	53.4	56.5	3.7	3.9	Rough surface
I	SL-P0.5	0.5	52.4	47.2	3.8	3.4	
	SL-P2.0	2.0	52.8	47.8	3.8	3.4	
II	SL-C30	1.0	50.7	33.7	3.7	2.7	
	SL-C70		52.3	69.6	3.7	4.9	
III	SL-Smooth		50.6	55.2	3.5	3.8	Smooth surface

σ_i: initial prestress level introduced to the interface between the old and new deck slabs; f_c': compressive strength of concrete and f_t: tensile strength of concrete

portant conditions in the bridge case have been considered in this study, consisting of the prestressing force and the supporting point condition.

The first is the prestressing force condition. In the real structure as shown in **Figs. 2a** and **b**, the compression at the new deck slab and subsequently at the interface between the old and new deck slab, due to prestressing in the upper PC cable, is externally transmitted through an interface between the precast rib and the new deck slab. The compression at the new deck slab is introduced by attaching the shear connectors in the precast ribs as shown in **Fig. 2c**. Theoretically, the tendons in the external PC members are being treated as the unbonded tendons. Therefore, it was reasonable in this study to use the unbonded PC rods to simulate the external compression force in the real structure. Moreover, to assure the full transfer of the prestressing force at the slab, the unbonded PC rods in this study were positioned at 275 mm from the center line of the slab as shown in **Fig. 2d**. This arrangement formed the angle θ of 33°40', which is specified by Japan Road Association 2012.

The second is due to the supporting point condition. In the real structure as shown in **Fig. 2a** and **b**, the slab tends to be fixed along the three directions; one comes from the old slab and the rest comes from the precast ribs. Hence, in the experimental study, the slabs were supported on three-line fixed supports as shown in **Fig. 2d**.

Based on the above conditions, all the specimens in this study were (1) subjected to prestressing force using unbonded PC rod and (2) supported on three-line fixed supports as shown in **Fig. 2d**.

b) Test specimens

Six specimens belonging to the three series were tested to investigate the effect of prestressing level, concrete strength of the deck new slab, and surface roughness of the interface (**Table 1**). **Figure 3** shows the details of the specimens. The slabs were scaled down according to half scale model with the geometrical parameters were 1500 mm long, 1225 mm wide and 100 mm thick. Each specimen consists of two parts and is cast at different times. The old slab is cast first followed by the new slab after seven days. To reproduce the rough surface, the old slab in all specimens, except for SL-Smooth, were intentionally roughened by using the retarder at the day before casting and spraying with high-pressure water after de-molding. Meanwhile, to reproduce the smooth surface in SL-Smooth, the new concrete was cast directly against the old concrete without any roughness treatment.

c) Material properties

The maximum size of course aggregate (G_{max}) was 10 mm. The design compressive strength (f_{cd}') of the old slab was fixed at 50 MPa, while f_{cd}' of the new slab varied at 30, 50, and 70 MPa. Cylinders with ϕ100x200 mm were cast from each concrete batch. Compressive and splitting tensile tests were conducted at the time of the loading test, as tabulated in **Table 1**. The diameters of rebars were 6, 10, and 16 mm with the average yield strength of 345.0, 392.8, and 386.0 MPa, respectively. The yield strength f_{py}, tensile strength f_{pu}, and elastic modulus E_{ps}, of the PC rods were 1171, 1268, and 2.01×10^5 MPa, respectively.

d) Parameters

Three parameters are investigated and are summarized in **Table 1**. The first series investigates the effect of the initial prestressing level (σ_i), which varies into SL-P0.5 (0.5 MPa), SL-P1.0 (1.0 MPa), and SL-P2.0 (2.0 MPa). The first series aims to evaluate the effect of initial prestressing level that will be introduced through the upper PC cable (**Figs. 1b** and **2a**). The second series comprises three specimens to examine the effect of the strength of the new deck slab. It varies from 30, 50, and 70 MPa in SL-C30, SL-P1.0, and SL-C70, respectively. The last series investigates the effect of surface roughness of the interface, which consists of rough (SL-P1.0) and smooth surface (SL-Smooth).

e) Instrumentations and test setup

A hydraulic jack with 3000 kN capacity was used to apply the vertical load. The magnitude of the applied load was measured using a load cell. Transducers were used to measure the deflections, and π-gauges were used to measure the joint opening (**Fig. 4a**). Several strain gauges were also attached to the steel bars and PC rods (**Fig. 4b**).

Figure 5 shows a photograph of the test. The deck slab was restrained at the supporting steel beams and fixed with steel bolts along the three edges. This is to reproduce the fixed constraints similar to those of real bridge deck slabs. The sizes of the steel beam and steel bolts were designed for adequate strength. Similar test meth-

ods were conducted by some previous researchers (El-Gamal *et al*. 2007; Chigira *et al*. 2007). Before testing, the slabs were prestressed using two unbonded PC rods and anchored at both ends of the slabs. A concentrated load was then applied to the new slab center by using a steel loading plate (100 mm x 250 mm). This loaded area was equivalent to the half scale of the footprint for the truck wheel load of 100 kN as specified by AASHTO 2007.

2.2 Nonlinear FEM analysis program

The finite element program DIANA (Ver. 9.5) was used to carry out the three-dimensional nonlinear FEM analysis. The concrete slabs were modeled with

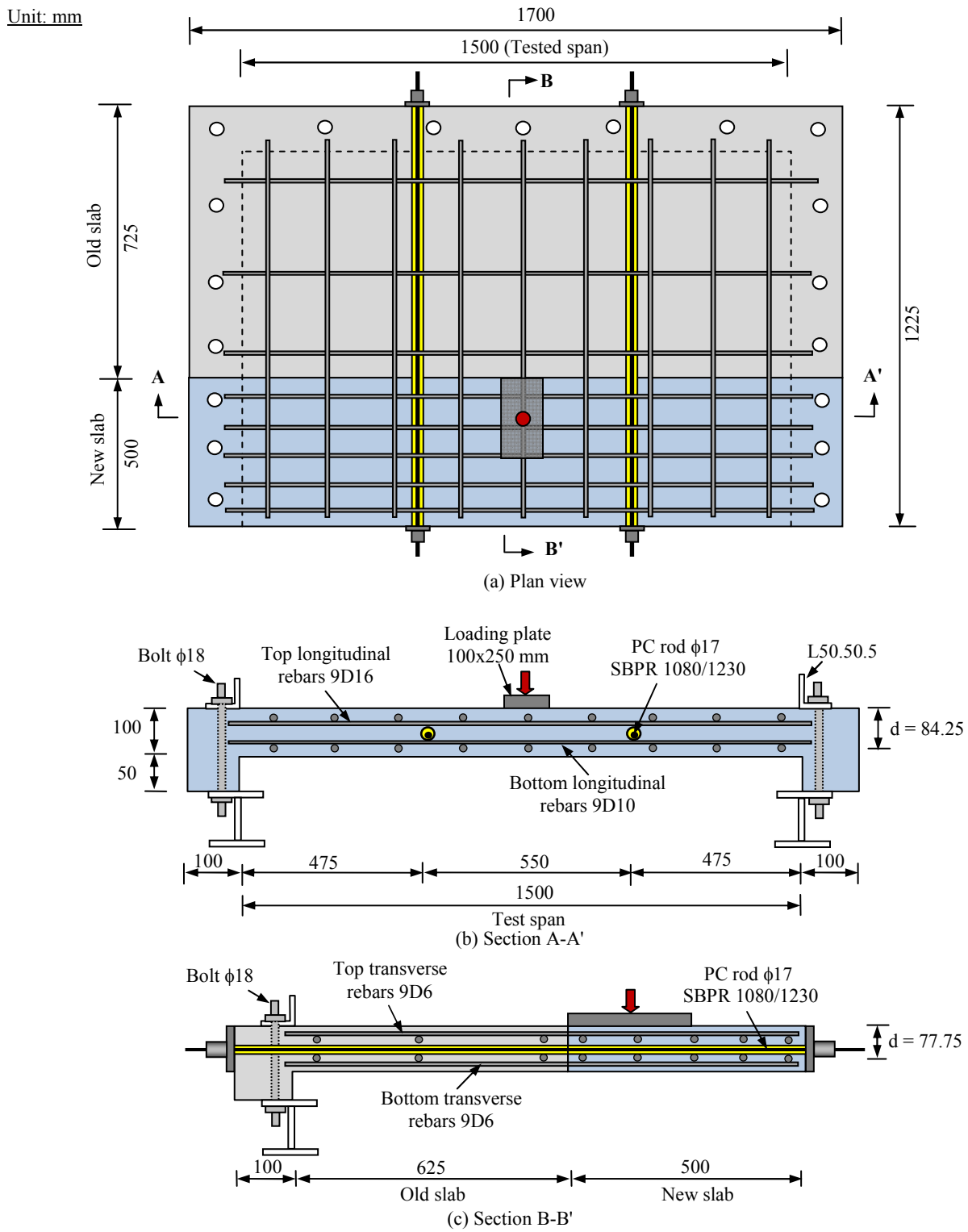

Fig. 3 Deck slab layout and reinforcement details.

20-noded isoparametric solid elements with the size of 50 mm as shown in **Fig. 6**. In this work, the crack bandwidth is taken as the characteristic length $h = \sqrt[3]{V}$ (V is the volume of the element).

The total strain fixed smeared crack model was applied for the crack model of concrete. The behavior of concrete in compression was modeled using the stress-strain relationship proposed by Thorenfeldt *et al.* (1987) as shown in **Fig. 7a**. The area below the softening part of the compressive stress-strain curve equals to G_c/h.

The compressive fracture energy G_c is difficult to measure due to strong dependence on the testing procedure, but it appears to be 100-500 times greater than the tensile fracture energy G_f (Eder *et al.* 2010). However, the failure load of the models analyzed in this study was largely insensitive to G_c around 250 G_F. After cracking, the tension-softening model proposed by Hordijk (1991) was used as the concrete constitutive model under tension as illustrated in **Fig. 7b**. The tensile fracture energy G_F was obtained according to JSCE Specification (2007):

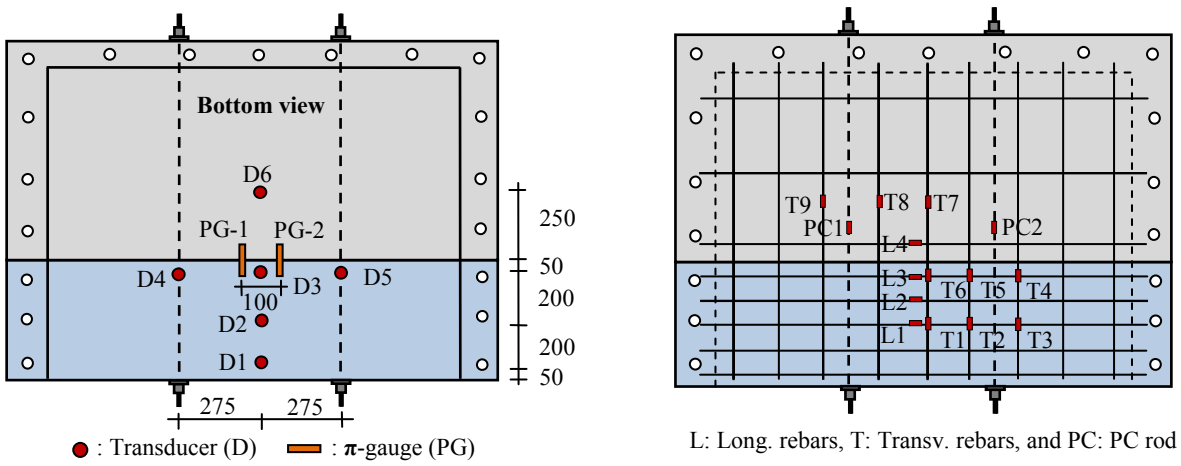

(a) Location of transducers and π-gauges (b) Location of steel gauges

Fig. 4 Measurement items.

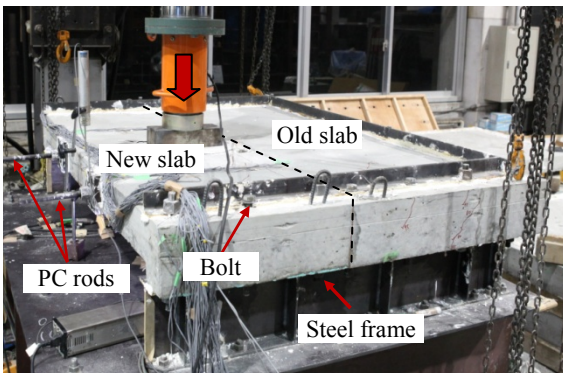

Fig. 5 Photograph of the test.

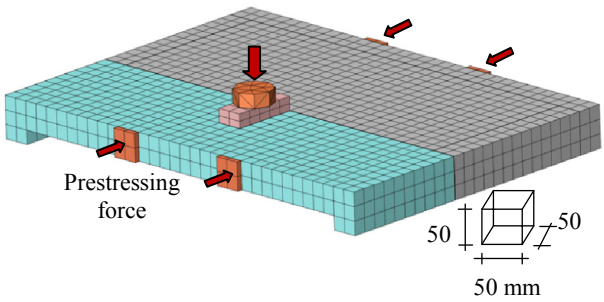

Fig. 6 Three-dimensional finite element mesh.

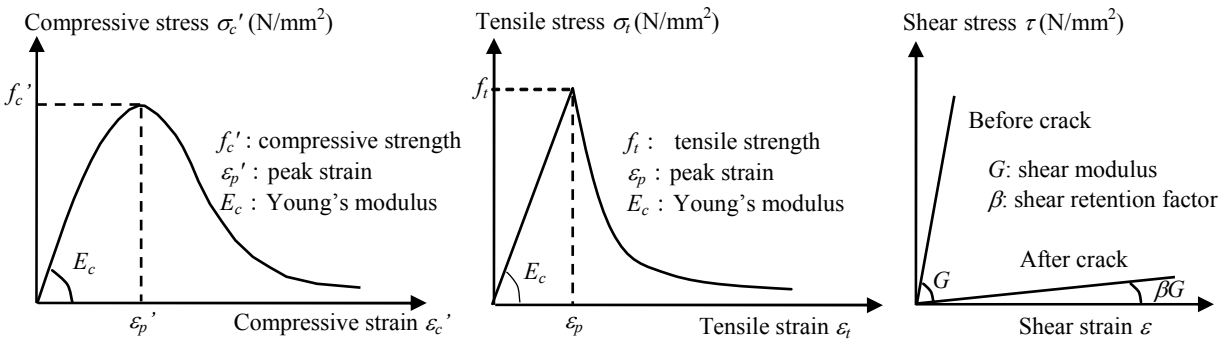

(a) Parabolic model considering fracture energy G_c (b) Hordijk model (c) Shear model

Fig. 7 The material model for concrete.

Table 2 Variables in Coulomb friction model.

Parameters	All slabs (except SL-P0.5 and SL-Smooth)	SL-P0.5	SL-Smooth
Normal stiffness, k_n (N/mm^3)	5 x 10^4	5 x 10^4	5 x 10^4
Tangential stiffness, k_t (N/mm^3)	5 x 10^4	5 x 10^4	5 x 10^4
Friction angle, tanϕ	1	1	0.7
Cohesion, c (N/mm^2)	1.93	1.0	1.93

$$G_F = 10(d_{\max})^{1/3} f_c'^{1/3} \quad \text{(N/m)} \tag{1}$$

where d_{max} is the maximum size of coarse aggregate (mm) and f_c' is the compression strength of the concrete (N/mm^2). For the shear model, the constant shear retention model with the value of shear retention factor β equal to 0.1 was applied (**Fig. 7c**).

Reinforcing bars are modeled by means of the embedded reinforcement element in DIANA system while the PC rods are modeled by means of unbonded model. A bilinear elasto-plastic constitutive model is used to appropriately represent the stress-strain relationship of reinforcing bars and PC rods.

The flat joint model is applied to reproduce the interface between two concrete parts. The flat joint model is composed of two-node interface element, with different constitutive laws depending on the geometry that elements were reproducing (Turmo *et al*. 2006). These constitutive laws were derived from the formulation proposed by AASHTO (2007). Coulomb friction model with and without cohesion has been selected for the interface element between two concrete parts and are presented in **Figs. 8a** and **b**, respectively.

The values adopted for the characterization of Coulomb friction model are presented in **Table 2**. The important properties of the interface element model are identified by the value of normal stiffness k_n and tangential stiffness k_t in the elastic stage. When an interface element is introduced in a finite element model, the major prerequisite is that no additional deformation be introduced in the elastic stage. For this reason, the values of initial stiffness k_n and k_t have to exhibit a sufficiently high value to reproduce the continuous geometry of segmental concrete beams before the joint opening (Turmo *et al*. 2006; Sivaleepunth *et al*. 2009). However, the values of initial stiffness have to be small enough to avoid numerical problems during analysis. Turmo *et al*. (2006) proposed the value of k_n and k_t of 5 x 10^4 N/mm^3 for a flat joint model based on the FEM model that is calibrated with the experimental test. Thus, the value of 5 x 10^4 N/mm^3 was also used in this study. Moreover, the value of friction angle ϕ is taken to be equal to the friction coefficient between two concrete surfaces μ proposed by AASHTO (2007), because the flat joint model was derived from the formulation proposed by this guideline. The other important value is the cohesion value (c). The cohesion values in **Table 2** are determined based on comparing between the experimental results and FEM analysis, such as load-deflection and load-joint opening curves that will be discussed in **Section 4.1**.

During the analysis, the prestressing force was applied by using the incorporated prestressing command in DIANA system at the first step. After the first step, the displacement control and the Quasi-Newton method was used in the iteration.

3. Experimental results and discussion

3.1 Cracking pattern and failure mode

Table 3 summarizes the experimental results. **Figure 9** presents the crack patterns of the tested slabs, in which the solid and dashed lines express the cracks on the top and bottom surfaces, respectively. SL-P2.0 had larger number of flexural cracks due to larger initial prestresssing level. Moreover, the flexural cracks from the old slab in SL-Smooth were disconnected at the interface due to lower shear transfer strength in the smooth surface. These indicate that both the prestressing level and surface roughness significantly influence the crack patterns of the slab.

Even though the number of flexural cracks was different in each slab, the final flexural cracks on the bottom surface of all slabs were similar with the typical flexural yield line pattern for the slab supported on three-line fixed supports. Meanwhile, the observed crack on the top

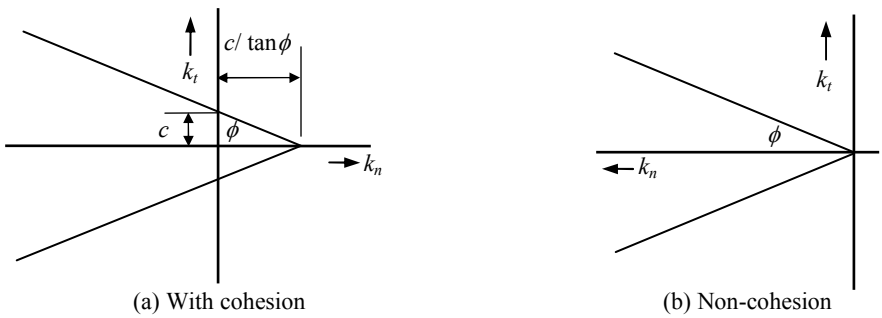

(a) With cohesion (b) Non-cohesion

Fig. 8 Coulomb friction model.

Table 3 Experimental results.

Specimen	P_{cr} (kN)	P_y (kN)		P_u (kN)	JO (mm)		δ (mm)		Failure mode
		Long. rebars	Transv. rebars		JO_y	JO_u	δ_y	δ_u	
SL-P1.0	63.0	87.0	103.0	141.0	0.15	2.14	4.16	22.9	Shear failure at the interface
SL-P0.5	53.0	75.0	71.0	109.0	0.17	1.36	4.61	16.2	
SL-P2.0	77.0	82.0	114.0	144.0	0.09	1.80	3.61	32.6	
SL-C30	55.0	83.0	107.0	136.0	0.07	2.35	4.06	27.8	
SL-C70	69.0	87.0	108.0	153.0	0.19	2.14	3.82	20.3	
SL-Smooth	55.0	83.0	102.0	139.0	0.14	2.37	3.77	27.7	

P_{cr}: first joint opening load; P_y: first yielding load at rebars; P_u: ultimate load; JO_y and JO_u: joint opening at P_y and P_u, respectively; δ_y and δ_u: displacement under the loading point (D3 transducer) at P_y and P_u, respectively

surface was similar with the typical shear failure of the interface between the old and new slabs. This crack pattern is clearly different from that of the typical punching shear failure. If the punching shear failure occurred, the punching cone can be observed on the surface of the slab. Hence, it can be concluded that the failure mode was the shear failure of the interface between the old and new slabs.

3.2 Load-joint opening and Load-deflection responses

Figure 10 shows the response of the load-average joint opening under the loading point. It was observed that the load-joint opening behaved similarly until the first joint opening load (P_{cr}), approximately at 53 kN to 77 kN (**Table 3**) or around 40% to 54% of the ultimate capacity. After that, the joint opening increased sharply up to the failure. Obviously, the behavior of load-joint opening in **Fig. 10a** was significantly different with the load-joint opening in **Figs. 10b** and **c**. This indicates that the effect of the initial prestressing level on the joint opening was more significant than concrete strength and surface roughness.

The responses of applied load-deflection are illustrated in **Fig. 11**. The displacements reported in this figure are the measured deflection under the loading point (D3 transducer in **Fig. 4a**). All slabs exhibited similar elastic behavior from the beginning until the first joint opening load (P_{cr}). After that, the slope of load-deflection curves gradually reduced until the failure. Finally, the load suddenly decreased because the interface has reached its ultimate strength. Similar with the joint opening, the effect of the initial prestressing level on the deflection was also more significant than the other parameters.

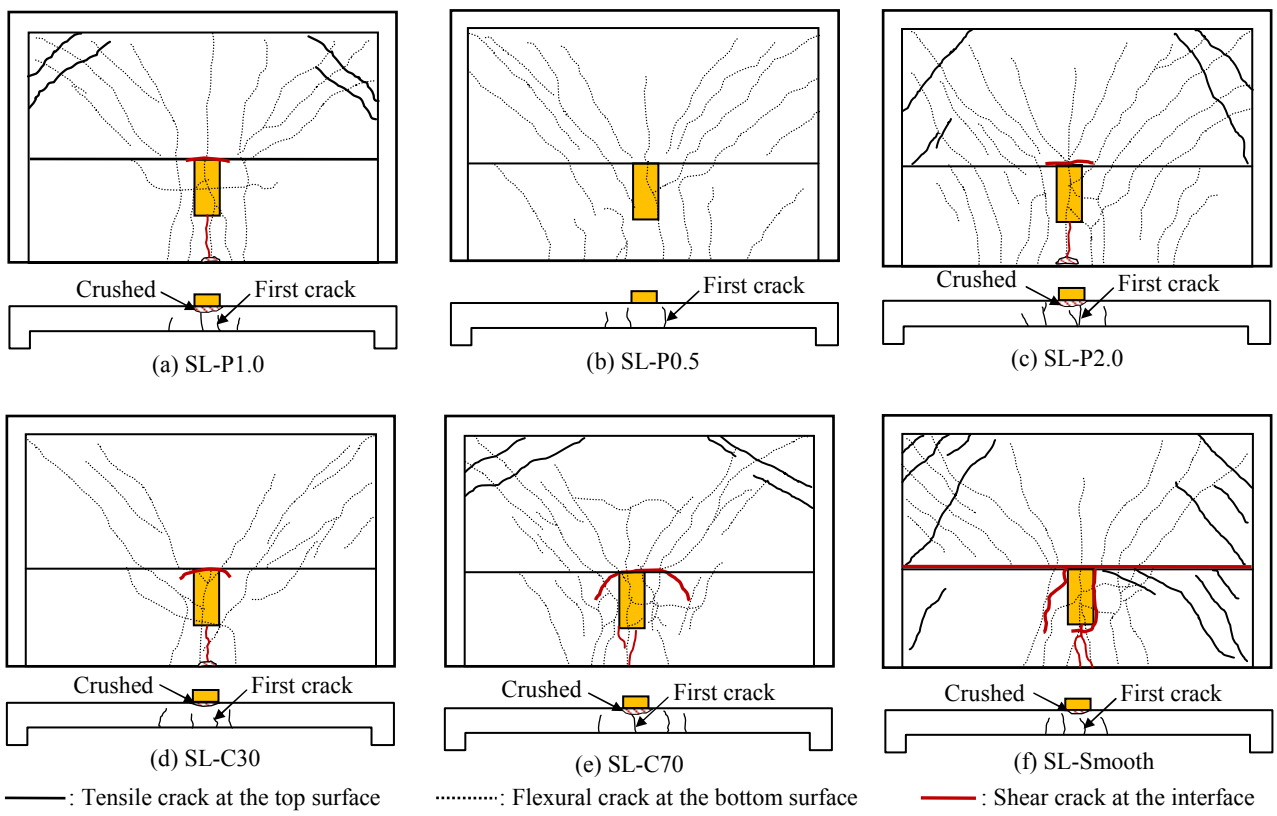

Fig. 9 Experimental crack patterns.

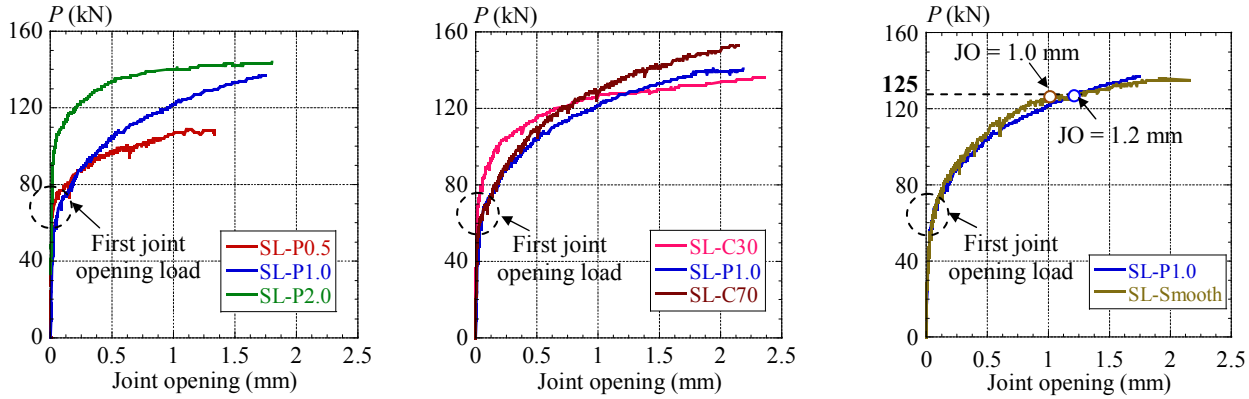

(a) Effect of prestressing level (Series-I) (b) Effect of concrete strength (Series-II) (c) Effect of surface roughness (Series-III)

Fig. 10 Load-average joint opening curves.

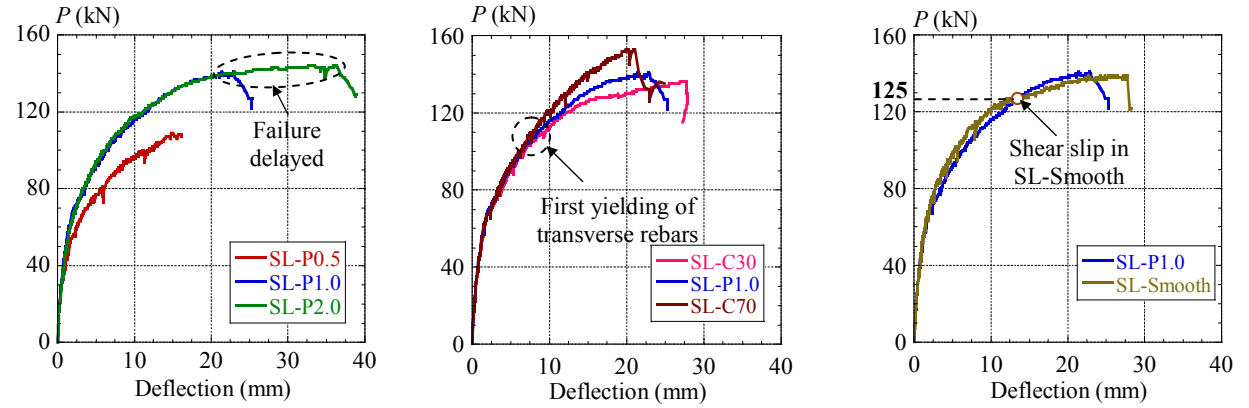

(a) Effect of prestressing level (Series-I) (b) Effect of concrete strength (Series-II) (c) Effect of surface roughness (Series-III)

Fig. 11 Load-deflection curves (D3 transducer).

3.3 Strain of rebars

a) Longitudinal rebars

Figure 12a shows the locations of the strain gauges attached in the longitudinal rebars with SL-P1.0 as reference. From **Fig. 12b**, it was seen that all the longitudinal rebars in the lower layer (LL) behaved in tension until the failure. The first yielding load (P_y) was observed at 87 kN or around 62% of the ultimate load. At the failure, all the LL rebars have yielded.

From **Fig. 12c**, it was observed that all the longitudinal rebars in the upper layer (LU) behaved in compression until the flexural cracks initiated on the bottom surface of the new slab at around 35 kN. After that, the behavior of LU changed to be tensioned, and finally yielded at the failure. Interestingly, the failure occurred just after the yielding of LU-3 rebars, which was located at 50 mm from the interface (**Fig. 12a**). This indicates that the failure was affected by the behavior of the LU rebars. Hence, in the design of the new slab, the reinforcement ratio of the LU rebars needs to be considered.

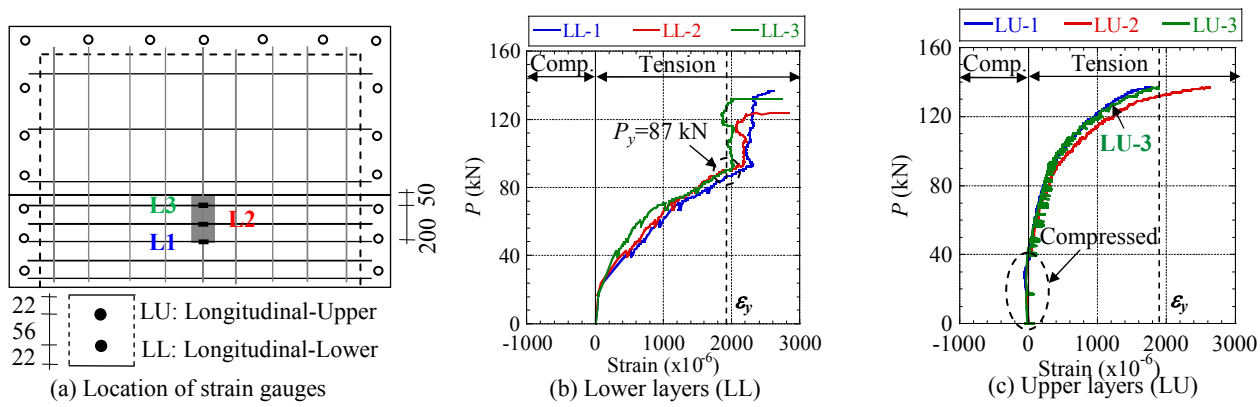

(a) Location of strain gauges (b) Lower layers (LL) (c) Upper layers (LU)

Fig. 12 Strain in the longitudinal rebars (SL-P1.0).

Table 4 Prestressing level at the cross-section of the interface and average prestressing force at PC rod.

Specimen	Initial (MPa)		Ultimate (MPa)		Δf_p (MPa)	$\Delta\sigma$ (MPa)	$\Delta f_p / f_{pe}$	P_u (kN)	$P_u/\sqrt{f_c'}$
	f_{pe}	σ_i	f_{ps}	σ_u					
SL-P1.0	327.2	0.82	436.2	1.10	109.0	0.27	0.33	141.0	18.8
SL-P0.5	161.4	0.41	240.0	0.60	78.6	0.20	0.49	109.0	15.7
SL-P2.0	641.8	1.62	877.6	2.21	235.8	0.59	0.37	144.0	20.8
SL-C30	329.4	0.83	516.8	1.30	187.4	0.47	0.57	136.0	-
SL-C70	326.0	0.82	463.4	1.17	137.4	0.35	0.42	153.0	-
SL-Smooth	330.6	0.83	401.8	1.01	71.2	0.18	0.22	139.0	18.7

f_{pe} and f_{ps}: the average PC rod stress at initial and ultimate load, respectively; σ_i and σ_u: the average prestress level of concrete at initial and ultimate load, respectively; Δf_p: average stress increment at PC rod; $\Delta\sigma$: the increment of average prestress level of concrete; P_u: ultimate capacity

b) Transverse rebars

Figure 13a presents the locations of strain gauges attached in the transverse rebars with SL-P1.0 as reference. Two strain gauges were attached at the same rebars, the one at 50 mm from the interface and the other at 250 mm from the interface. It was observed in **Fig. 13b** that all the transverse rebars in the lower layer (TL) behaved in tension until the failure. The first yielding load (P_y) was observed in TL-6 (under the loading point) at the load of 103 kN (**Table 3**), or around 86% of the failure load. At the failure, all the TL rebars at 50 mm from the interface (TL-4, TL-5 and TL-6) yielded. However, all the TL rebars at 250 mm from the interface (except for TL-2) have not yielded at the failure. This indicates that the measured strain of the TL rebars varied along its length and was the highest at the interface.

From **Fig. 13c**, it was observed that all the transverse rebars in the upper layer (TU) behaved in compression at the beginning until the opening of joint (P_{cr}). The first joint opening was observed in TU-6 at the load of 63 kN. After that, the behavior of all TU rebars changed to be tensioned until the failure. Interestingly, the failure occurred just after the yielding of TU-6, which was located under the loading point. This result supports the conclusion in **Section 3.1** that the interface shear failure observed in this study was governed by the loss of confinement of the transverse rebars in the upper layer under the loading point. According to Maekawa *et al.* (1997), this phenomenon is the most common failure criterion for RC interface.

3.4 Effect of prestressing level

The effect of the initial prestressing level (σ_i) was investigated in SL-P0.5 (0.5 MPa), SL-P1.0 (1.0 MPa) and SL-P2.0 (2.0 MPa) and is presented in **Table 1**. The responses of load-joint opening and load-deflection are illustrated in **Figs. 10a** and **11a**, respectively. The summary of the measured data, which includes the first joint opening load (P_{cr}), the ultimate load (P_u), and the midspan deflection at the ultimate (δ_u), is tabulated in **Table 3**. The stress increment at the PC rods (Δf_p) is tabulated in **Table 4**. The value of Δf_p is calculated by subtracting the initial prestressing stress, f_{pe}, from the ultimate prestressing stress, f_{ps}. In this study, the tensile stress in all unbonded PC rods never reached its nominal yield strength at the failure.

The prestressing level influenced the first joint opening load (P_{cr}). From **Table 3**, SL-P0.5 showed the lower P_{cr} (53 kN); and on the other hand, SL-P2.0 showed the larger P_{cr} (77 kN). This indicates that the first joint opening load is directly influenced by the prestressing level. The higher the prestressing level, the higher the first joint opening load can be observed. This is because the prestressing level acts as a clamping stress, which resulted in a frictional force on the interface and hence, delayed the opening of the joints.

The responses of load-deflection are shown in **Fig. 11a**. It was observed that once the joints opens, approximately at 53 kN to 77 kN (**Table 3**), the stiffness of the slab was strongly influenced by the prestressing level. The higher the prestressing level, the smaller the deflection at the

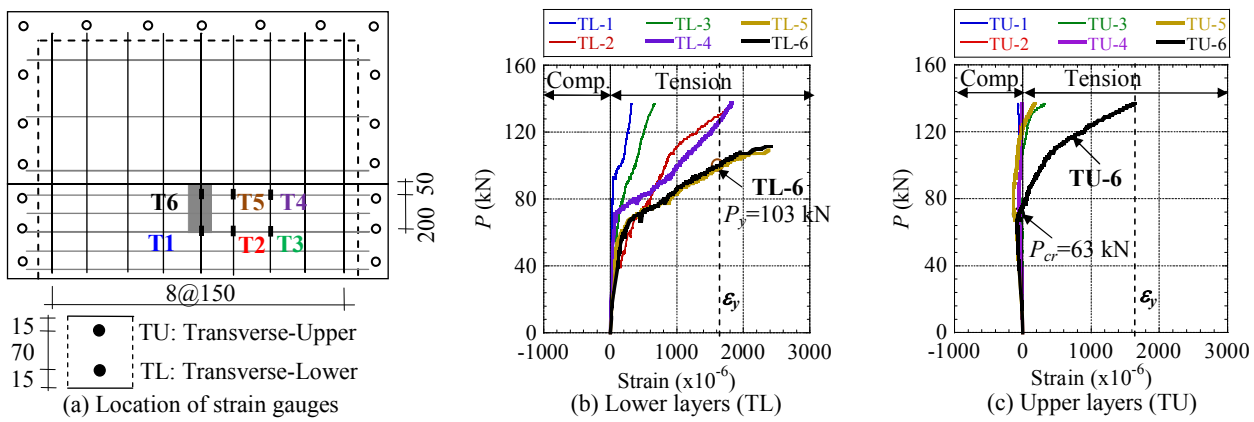

Fig. 13 Strain in the transverse rebars (SL-P1.0).

same load level can be observed. On the contrary, the measured deflection at the failure (δ_u) increased with the increase in the prestressing level. It was seen in **Table 3** that SL-P0.5 showed smaller δ_u (16.2 mm), while SL-P2.0 showed larger δ_u (32.6 mm). According to Haskett *et al*. (2011), greater prestressing level across the interface promotes greater shear transfer capacity and delays the failure.

The measured concrete strains at the top fiber of the interface in SL-P0.5 and SL-P1.0 are presented in **Fig. 14b**. The strain gauge was attached perpendicular to the interface, exactly at 137.5 mm from the slab center (**Fig. 14a**). At the same strain level, SL-P1.0 showed higher compression force which was developed at the top fiber of the interface than that of SL-P0.5. For a compression force value lower than the one necessary for resisting the applied load, larger displacement could occur once the joint opened. On the other hand, for a compression force value larger than the one necessary for resisting the applied load, smaller displacement was expected once the joint opened. These results suggested that the prestressing level larger or equal to 1.0 MPa is more capable of resisting the sliding shear stress than that the prestressing level lower or equal to 0.5 MPa.

All slabs failed in shear of the interface between the old and new slabs. The ultimate capacities of SL-P0.5, SL-P1.0, and SL-P2.0 were 109 kN, 141 kN, and 144 kN, respectively (**Table 3**). This indicates that larger prestressing level across the interface facilitates greater ultimate capacity. However, comparing SL-P1.0 with SL-P2.0, it was seen that the ultimate capacity in these slabs was almost similar even though the prestressing level was increased from 1.0 to 2.0 MPa. This could be caused by the difference in the concrete strength (f_c'). Thus, to make it independent of the concrete strength, the obtained ultimate capacity was divided with the square root of concrete compressive strength ($P_u/\sqrt{f_c'}$). P_u is the ultimate capacity (kN) and f_c' is the concrete compressive strength (N/mm^2).

The divided ultimate capacities $P_u/\sqrt{f_c'}$ of SL-P0.5, SL-P1.0, and SL-P2.0 were 15.9, 18.8 and 20.8, respectively and are shown in **Fig. 15a**. This indicates that the increase in the prestressing level from 0.5 to 1.0 MPa can improve the ultimate capacity (16.5%) more effectively than the increase in the prestressing level from 1.0 to 2.0 MPa (10.6%). This is in agreement with Hwang *et al*. (2010) and Clement *et al*. (2013) who concluded that the ultimate capacity is not increased proportionally with the initial prestressing level. The positive influence of the prestressing level tended to reduce with the increase in the initial prestressing level. One of the reasons is that the ratio of the stress increment in the unbonded PC rod ($\Delta f_p/f_{pe}$) decreased with the increase in the prestressing level. As tabulated in **Table 4**, $\Delta f_p/f_{pe}$ ratios reduced from

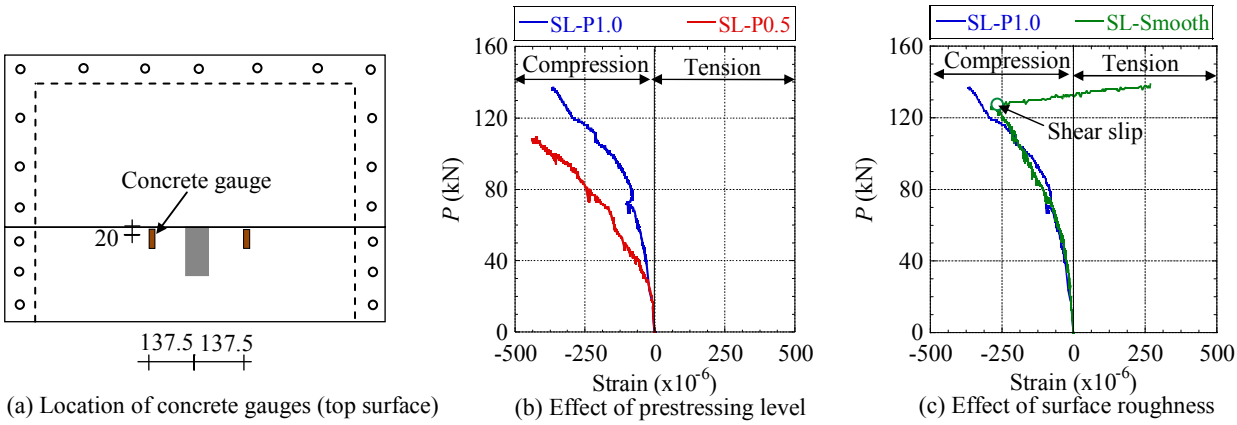

(a) Location of concrete gauges (top surface) (b) Effect of prestressing level (c) Effect of surface roughness

Fig. 14 Behavior of concrete gauge perpendicular to top fiber of the interface.

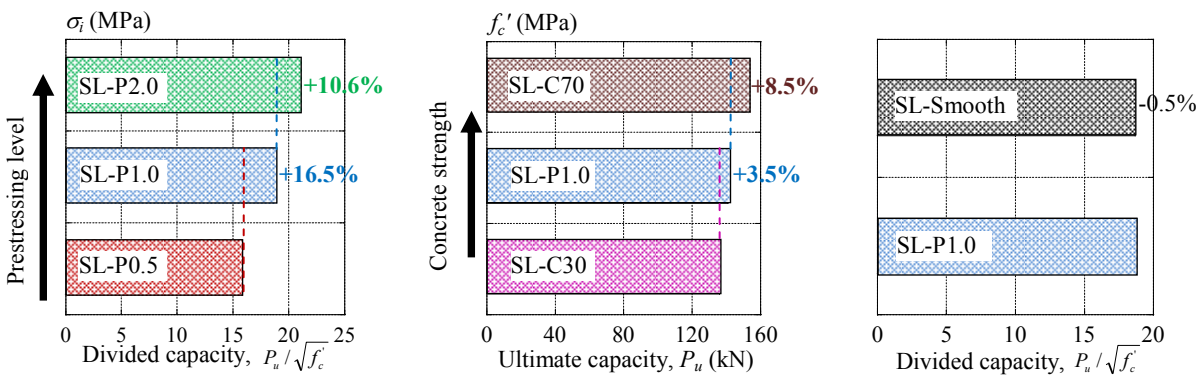

(a) Effect of prestressing level (b) Effect of concrete strength (c) Effect of surface roughness

Fig. 15 Ultimate capacity.

0.49 (0.5 MPa) to 0.37 (2.0 MPa). In the shear transfer mechanism, the ultimate capacity of the interface is dependent on the stress increment in the PC rod. The higher the tensile stresses induced to the PC rod, the higher the total shear resistance that can be transferred to the interface.

Eventually, from the above results, the summary of the effect of the prestressing level can be drawn in four main points: (a) The first joint opening load is directly influenced by the prestressing level. The higher the prestressing level, the higher the first joint opening load can be obtained. (b) The increase in the prestressing level decreases the deflection at the same load level and on the other hand, it increases the deflection at the ultimate load. (c) The ratio of the stress increment in the unbonded PC rod reduces with the increase in the prestressing level. (d) The positive influence of the prestressing level tends to decrease with the increase in the prestressing level.

3.5 Effect of concrete strength

The effect of the concrete strength (f_c') was investigated in SL-C30, SL-P1.0 and SL-C70, having the concrete strength of 33.7, 56.5 and 69.6 MPa, respectively. As shown in **Table 3**, the first joint opening load (P_{cr}) of SL-C30, SL-P1.0, and SL-C70 were 55.0, 63.0, and 69.0 kN, respectively, and the deflections at the failure (δ_u) of those slabs were 27.8, 22.9 and 20.3 mm, respectively. These indicate that when the concrete strength of the new deck slab increased, the first joint opening load increased and on the other hand, the deflection at the failure decreased. The first joint opening load increased in higher concrete strength due to the higher aggregate interlocking force which was produced from the bonding strength between two concrete faces. Meanwhile, the deflection at the failure decreased in higher concrete strength is due to the higher stiffness of the slabs.

Since the increase in the PC rods stress depended on the deformation of the full member, the smaller the joint opening and the deflection, the smaller ratios of the stress increment and the initial stress ($\Delta f_p/f_{pe}$) can be observed. As shown in **Table 4**, SL-C30 registered larger $\Delta f_p/f_{pe}$ ratio of 0.57 due to the larger joint opening and deflection at the failure. Slab SL-C70, on the other hand, registered lower $\Delta f_p/f_{pe}$ ratio of 0.42 due to the smaller joint opening and deflection at the failure.

The ultimate capacities P_u of SL-C30 (136 kN), SL-P1.0 (141 kN) and SL-C70 (153 kN) are presented in **Figure 15b**. SL-C30 showed lower ultimate capacity due to lower concrete strength. On the other hand, SL-C70 showed larger ultimate capacity due to larger concrete strength. Agreed with Rahal *et al*. (2016), the concrete strength has a considerable effect on the ultimate capacity. However, similar with the prestressing level, the ultimate capacity also did not increase proportionally with the concrete strength. The comparison between the concrete strength f'_c and the ultimate capacity P_u of SL-C30 and SL-P1.0 showed the increase in f'_c of 1.68 times and P_u of 3.5%. However, the comparison between f'_c and P_u of SL-P1.0 and SL-C70 showed the increase in f'_c of 1.23 times and P_u of 8.5%. This indicates that the positive influence of the concrete strength became more significant when the concrete strength of the new slab (loaded slab) was larger than the concrete strength of the old slab. This is reasonable due to the flexural capacity of the new slab (loaded slab) also affected the ultimate capacity as it was discussed in **Section 3.3**.

From the above results, the summary of the effect of the concrete strength of the new deck slabs can be drawn in three main points: (a) The first joint opening load and the deflection at the failure is directly influenced by the concrete strength. The higher the concrete strength, the higher the first joint opening load and on the other hand, the smaller the deflection at the failure can be observed. (b) The stress increment at the unbonded PC rod decreased with the increase in the concrete strength. (c) The ultimate capacity of the interface increased with the increase in the concrete strength.

3.6 Effect of surface roughness

The effect of the surface roughness was investigated in SL-P1.0 (rough) and SL-Smooth (smooth). The responses of load versus joint opening are presented in **Fig. 10c**. It was seen that the joint opening of SL-P1.0 was almost similar with SL-Smooth until the first joint opening load (P_{cr}), which occurred at 63 kN and 55 kN, respectively (**Table 3**). Beyond the P_{cr}, the difference between SL-P1.0 and SL-Smooth could be clearly observed, whereas the magnitude of the joint opening in SL-P1.0 was greater than that of SL-Smooth at the same load level. For instance, at the load of 125 kN, the measured joint openings in SL-P1.0 and SL-Smooth were 1.2 mm and 1.0 mm, respectively (**Fig. 10c**). This is because the joint opening in SL-P1.0 was concentrated around the loading point (**Fig. 9a**) while the joint opening in SL-Smooth was propagated into the whole of the interface (**Fig. 9f**).

To explain the above behavior, the responses of load-concrete strain at the top fiber of the interface are presented in **Fig. 14c**. The strain gauge was attached perpendicular to the interface, exactly at 137.5 mm from the slab center (**Fig. 14a**). Obviously, the top fiber of the interface tended to be compressed from the beginning up to 125 kN. After that, the shear resisting mechanism of the interface significantly changed. When the interface became rough, the top fiber of the interface was still able to form the compression fiber until the failure. However, when the interface became smooth, the compressive force gradually reduced and turned into tension. Hence, the joint opening propagated along the smooth interface and finally produced a significant shear slip as shown in **Fig. 16**. At the failure, SL-Smooth registered greater deflection (27.7 mm) compared with that of SL-P1.0 (22.9 mm) as shown in **Table 2**.

Table 3 tabulates the ultimate capacities of SL-P1.0 (141 kN) and SL-Smooth (139 kN). In order to make it independent of the concrete strength, the obtained ulti-

mate capacity was divided by the square root of concrete compressive strength ($P_u / \sqrt{f_c'}$). P_u is the ultimate capacity (kN) and f_c' is the concrete compressive strength (N/mm^2). Thus, $P_u / \sqrt{f_c'}$ of SL-P1.0 and SL-Smooth were 18.8 and 18.7, respectively (**Fig. 15c**). It indicates that the ultimate capacity was almost same as the surface roughness changed from rough to smooth surface.

The above results were contradicted by the general agreement for the concrete-to-concrete interface under direct-shear test (Randl 2013; Niwa *et al*. 2016), which concluded that as the degree of roughness of a particular surface increases; the ultimate capacity also increases significantly. The different results in this study can be explained as follows. For the PC deck slab subjected to a concentrated load (**Fig. 17a**), the width of the loading plate was much smaller than the total width of the interface. Hence, the compressive stress will be concentrated only in the particular part of the interface, exactly around the loading point. Moreover, due to the two-way slab interaction, the contribution of the loaded slab (new slab) is also significant on the ultimate capacity as it was discussed in **Section 3.5**. Therefore, in the case of PC deck slab under a concentrated load, the ultimate capacity will be determined by two factors, the one from the shear capacity of the interface and the other from the flexural capacity of the new slab (loaded panel). On the other hand, in the case of the direct-shear test in **Fig. 17b**, the strip specimen representing the deck slab section will be used. It is seen in this figure that the width of the loading point is equal to the total width of the interface. The shear stress will be localized at the total area of the interface and consequently, the interface becomes the weakest point than the loaded slab (new slab). Therefore, in the case of the direct-shear test, the ultimate capacity can be determined by the ultimate capacity of the interface between the old and new slabs.

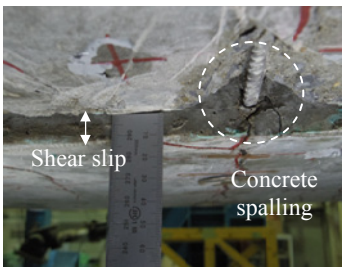

Fig. 16 Shear slips in SL-Smooth (bottom surface).

Eventually, from the above results, the summary of the effect of the surface roughness can be drawn in two main points: (a) the first joint opening load, the joint opening at the same load level, and the deflection at the failure are directly influenced by the surface roughness. The higher the degree of roughness of a particular surface, the higher the first joint opening load and the joint opening at the same load level; and on the other hand, the smaller the deflection at the failure can be observed. (b) The variation in surface roughness does not show any remarkable influence on the ultimate capacity. However, it must be noted that the results in this study were limited to the case of PC deck slab supported on three-sides and subjected to a concentrated load immediately adjacent to the interface.

4. Comparison of experiment and analysis

4.1 Nonlinear FEM analysis

Since it was observed from the experiment that the prestresing level had large influence on the opening of joint, the nonlinear FEM analysis was used in this study in order to investigate its behavior on the joint opening, the failure mode, and the principal strain flow. FEM analysis was also used to check the values adopted for the characterization of the Coulomb friction model which are presented in **Table 2**.

The nonlinear FEM analyses for SL-P0.5 and SL-P1.0 were conducted first to check the feasibility of the FEM model. After that, the FEM analyses for remaining slabs were performed. The validation of FEM analysis was examined by comparing the analytical results with the experimental results as illustrated in **Figs. 18a** and **b**. It can be observed that FEM analysis can predict not only the load-deflection response, but also the load-joint opening response. The ratios of the experimental to the analytical capacity (P_{EXP}/P_{FEM}) of SL-P1.0 and SL-P0.5 were 1.02 and 0.98, respectively (**Table 5**).

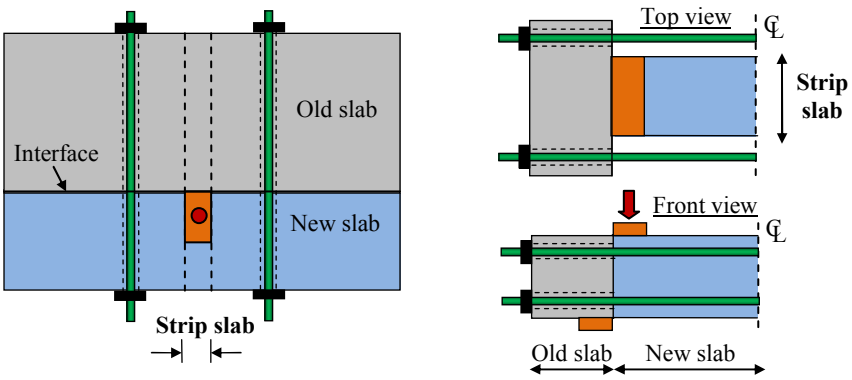

(a) PC slab under concentrated load (b) Direct shear test (Niwa et al. 2016)

Fig. 17 Behavior of PC slab under concentrated load vs. direct shear test.

The second objective of FEM analysis was to confirm the experimental failure mode. The experimental crack pattern on the bottom surface of SL-P1.0 (reference slab) was compared with the contour figure of principal strain at the peak load as shown in **Figs. 19a** and **b**, respectively. According to **Section 3.1**, the failure mode was the shear failure of the interface between the old and new slabs, in which the shear cracks developed at the interface (**Fig. 19a**). The development of the shear cracks at the interface can be also confirmed in FEM analysis, in which the concentrated principal strain was observed near the

Table 5 Ultimate capacity of experiment and analysis.

Specimen	P_{EXP} (kN)	P_{FEM} (kN)	P_{EXP} / P_{FEM}
SL-P1.0	141.0	138.0	1.02
SL-P0.5	109.0	112.0	0.98
SL-P2.0	144.0	140.1	1.03
SL-C30	136.0	133.5	1.02
SL-C70	153.0	149.5	1.02
SL-Smooth	139.0	131.1	1.06
Mean			1.02
Coefficient of Variation (C.V.)			2.9

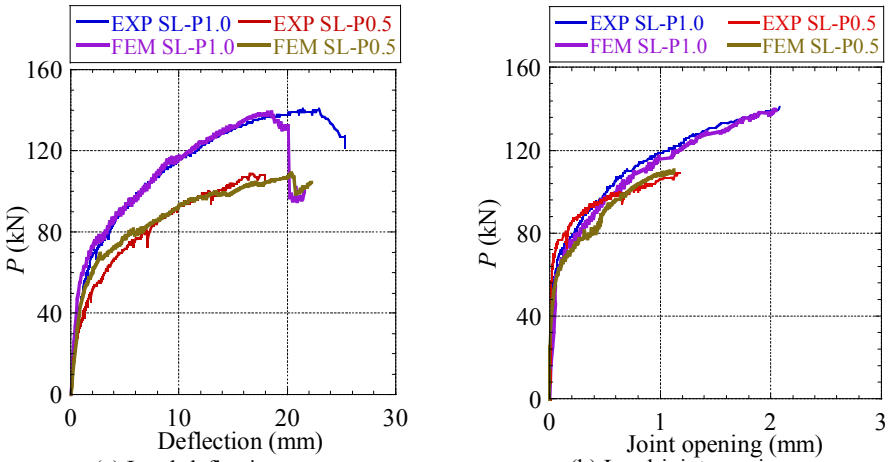

(a) Load-deflection curves (b) Load-joint opening curves

Fig. 18 Experiment vs. FEM analysis.

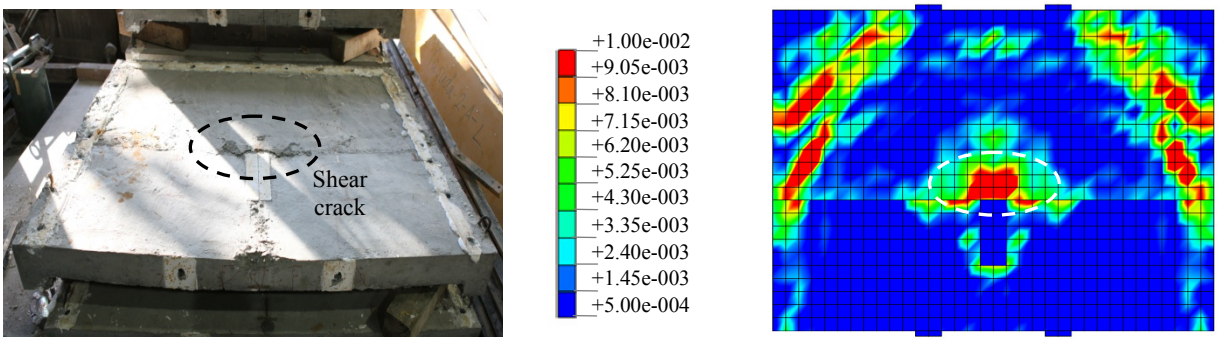

(a) Experimental crack pattern (b) FEM analysis

Fig. 19 Principal tensile strain on the top surface of SL-P1.0.

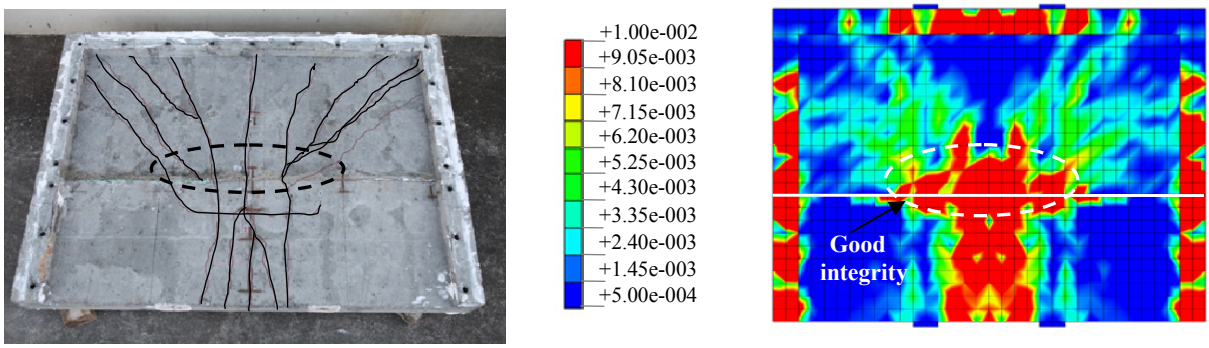

(a) Experimental crack pattern (b) FEM analysis

Fig. 20 Principal tensile strain on the bottom surface of SL-P1.0.

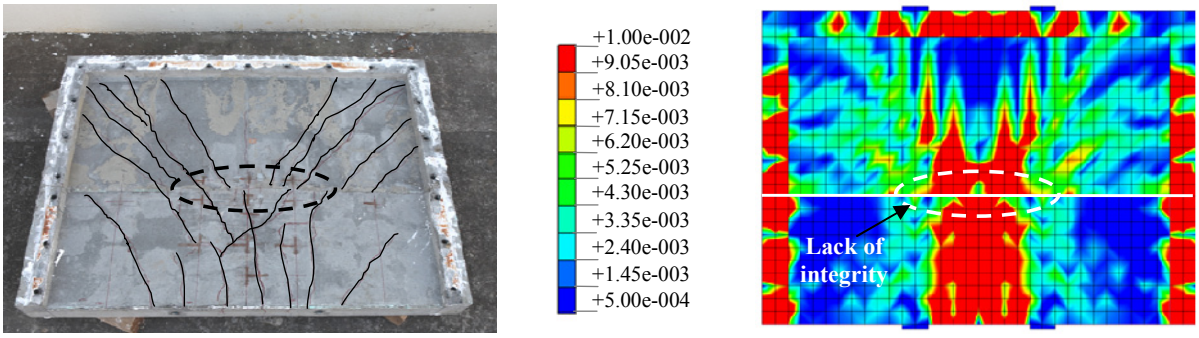

(a) Experimental crack pattern (b) FEM analysis

Fig. 21 Principal tensile strain on the bottom surface of SL-P0.5.

loading point (**Fig. 19b**).

In addition, since it was observed from the experiment that the amount of initial prestressing level affected the interface shear transfer, the comparison of the experimental crack patterns and the contour figures of principal strain at the peak load on the bottom surface of the SL-P1.0 and SL-P0.5, are presented in **Figs. 20** and **21**, respectively. According to **Figs. 20** and **21**, it was observed that the experimental crack patterns in both slabs had similarity with the contour figure of the principal strains, in which several flexural cracks can be observed on the bottom surface of the slabs. Also two other tendencies can be observed in **Figs. 20** and **21**. First, if the initial prestressing level was larger or equal to 1.0 MPa, the contour figures of principal strain could flow continuously across the interface (**Fig. 20b**). Second, if the initial prestressing level was lower or equal to 0.5 MPa, the contour figures of principal strain could not flow across the interface (**Fig. 21b**). In agreement with the experiment, FEM analysis also showed that the prestressing level of larger or equal to 1.0 MPa was more capable to resist the sliding shear stress than the prestressing level of lower or equal to 0.5 MPa.

After checking the feasibility of FEM model in SL-P1.0 and SL-P0.5, FEM analyses for the remaining slabs were conducted and are summarized in **Table 5**. The values used in the interface model are tabulated in **Table 2**. Again, FEM analyses showed a good agreement with the experiment. The ratios P_{EXP}/P_{FEM} varied from 0.98 to 1.06, with a coefficient of variation of 2.9% (**Table 5**).

In **Section 4.2**, the experimental ultimate capacities will be compared with the predicted ultimate capacities by using the existing guidelines. The total area of the interface (A_c) is required to calculate the shear capacity of the interface in the guidelines. From **Figs. 19**, **20** and **21**, it was observed that only some parts of the interface cracked when the shear failure occurred at the interface. Thus, the area of the interface for this study cannot be assumed as the total area of the interface, but it should be assumed as the effective area (A_{eff}). Since the values for constant in each design guideline were separated based on the roughness degree of the interface, the contour figures of the principal strain at the cross section of the interface for the rough surface (SL-P1.0 as representative) and smooth surface (SL-Smooth) have been presented in **Figs. 22a** and **b**, respectively. According to the shear-friction theory, the shear failure of the interface will occur after the yielding of the rebars crossing the interface (transverse rebars). Thus, the validation of the effective area from FEM analysis was made by comparing the number of the transverse rebars which have yielded at the failure. It was observed in **Fig. 13** that a total of four transverse rebars which have yielded at the failure in the rough surface (SL-P1.0). Meanwhile, a total of six transverse rebars which have yielded at the failure in the smooth surface (SL-Smooth). According to these observations, the effective area of the interface (A_{eff}) for the rough and smooth surface was proposed as a trapezoidal shape and is illustrated in **Figs. 22a** and **b**, respectively.

4.2 Predicted shear capacity

Since the experimental failure mode was a shear failure at the interface, the experimental shear capacities were compared with predicted shear capacities using JSCE Specification (2007), AASHTO (2007), and *fib* Model Code 2010 (2013). The shear capacity predicted by these guidelines was considered without partial safety factors.

Based on JSCE Specification, the design capacity for shear transfer P_u was computed using the following equations:

$$P_u = (\tau_c + p\tau_s \sin^2\theta - \alpha p f_y \sin\theta\cos\theta)A_c + P_k \quad (2)$$

$$\tau_c = \mu f_c'^b (\alpha p f_y - \sigma_n)^{1-b} \quad (3)$$

$$\tau_s = 0.08 f_y / \alpha \quad (4)$$

$$\alpha = 0.75\{1 - 10(p - 1.7\sigma_n / f_y)\} \quad (5)$$

where

p: reinforcement ratio ($p = A_s/A_c$)

A_s: area of reinforcement crossing the interface

A_c: area of the interface

θ: angle between interface and reinforcement at the interface ($\theta = 90^\circ$ in this study)

f_y: yield strength of reinforcement

P_k: shear capacity of shear key (P_k=0 in this study)

μ: coefficient of friction (μ=0.45 in this study)

σ_n: average normal compressive stress acting on the interface

b: coefficient representing configuration of planes (For segmental joint, b=0.5).

AASHTO provision gives the following design formula to estimate the nominal shear resistance of interface P_u:

$$P_u = cA_c + \mu(A_s f_y + N_c') \tag{6}$$

but not greater than the lesser of Eqs. (7) and (8).

$$P_u \le \kappa_1 f_c' A_c \tag{7}$$

$$P_u \le \kappa_2 A_c \tag{8}$$

where

c: cohesion factor (0.28 ksi or 1.93 MPa for rough, and 0.025 ksi or 0.172 for smooth)

N_c: compressive force normal to the interface

κ_1: friction of the concrete strength to resist the interface shear (**Table 6**)

κ_2: limiting the interface shear resistance (**Table 6**)

μ: coefficient of friction (**Table 6**).

In *fib* MC2010, the shear resistance of the interface τ_u was evaluated by the following equation:

Table 6 Values for constant in AASHTO and *fib* MC2010.

Codes	Surface roughness	τ_c	μ	κ_1	κ_2
AASHTO	Smooth	-	0.6	0.2	0.8
	Rough	-	1.0	0.3	1.8
MC2010	Smooth	0.5-1.5	0.5-0.7	0.5	1.1
	Rough	1.5-2.5	0.7-1.0	0.5	0.9

$$\tau_u = \underbrace{\tau_c}_{\text{Interlock}} + \underbrace{\mu(\sigma_n + \kappa_1 \rho f_y)}_{\text{Friction}} + \underbrace{\kappa_2 \rho \sqrt{f_{c,cube} f_y}}_{\text{Dowel action}} \le \beta v f_{c,cube} \tag{9}$$

where

τ_c: interlocking strength (**Table 6**)

κ_1: interaction factor of reinforcement due to simultaneous bending of rebars (**Table 6**)

κ_2: interaction factor for the dowel action (**Table 6**)

$f_{c,cube}$: cube compressive strength ($f_{c,cube}$ = $f_{c,cylinder}$ /0.85)

β: coefficient allowing for angle of diagonal concrete strut (0.5 for rough and 0.4 for smooth)

v: reduction factor for strength of diagonal concrete strut, which is calculated by Eq. (10).

$$v = 0.55\left(30/f_{c,cube}\right)^{1/3} \le 0.55 \tag{10}$$

It must be noted that the design guidelines assume the area of the interface as the total area of the interface

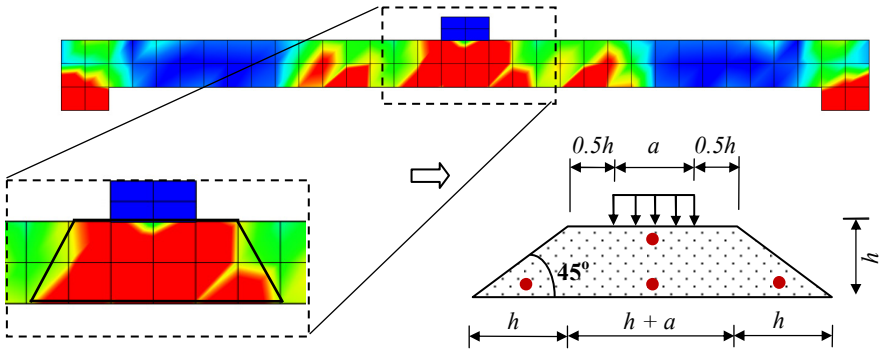

(a) Rough surface (SL-P0.5, SL-P1.0, SL-P2.0, SL-C30 and SL-C70)

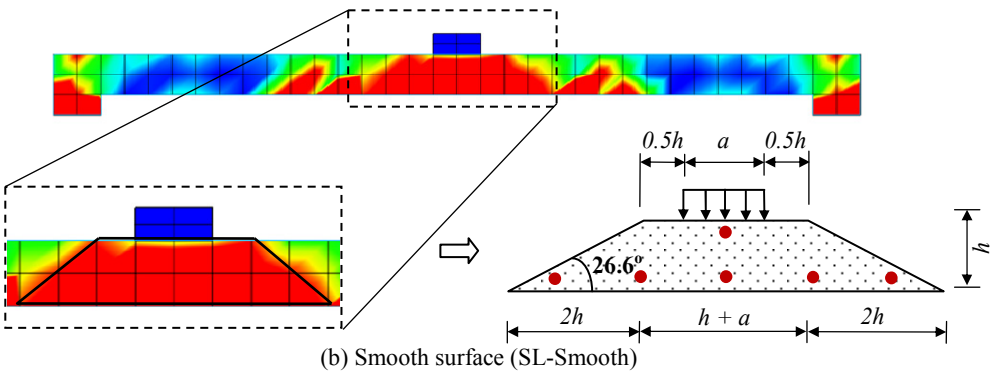

(b) Smooth surface (SL-Smooth)

h: thickness of the slab; a: length of rectangular concentrated loading; : transverse rebars which have yielded at the failure

Fig. 22 Effective area of the interface (A_{eff}).

Table 7 Comparison of experiment and calculation.

Specimen	A_{eff} (mm^2)	A_s (mm^2)	σ_u (MPa)	P_{EXP} (kN)	JSCE		AASHTO		*fib* MC2010	
					P_{CAL} (kN)	P_{EXP} / P_{CAL}	P_{CAL} (kN)	P_{EXP} / P_{CAL}	P_{CAL} (kN)	P_{EXP} / P_{CAL}
SL-P1.0	25 000	4D6 (126.7)	1.10	141.0	135.6	1.04	122.0	1.16	129.9	1.09
SL-P0.5			0.60	109.0	106.5	1.02	102.3	1.07	107.8	1.01
SL-P2.0			2.21	144.0	142.1	1.01	142.5	1.01	140.4	1.02
SL-C30			1.30	136.0	126.9	1.07	119.8	1.14	123.6	1.10
SL-C70			1.17	153.0	133.2	1.15	132.9	1.15	130.7	1.17
SL-Smooth	30 000	6D6 (190.1)	1.01	139.2	128.1	1.09	127.1	1.09	133.2	1.04
Mean						1.06		1.11		1.07
Standard deviation						0.05		0.05		0.05
Coefficient of Variation (C.V.)						4.3		4.7		5.0

A_{eff}: effective area of the interface; A_s: total area of the transverse rebars which have yielded at the ultimate load; σ_u: average prestressing level at the ultimate load; P_{EXP}: ultimate capacity from experiment; P_{CAL}: ultimate capacity from calculation

(A_c=150 000 mm^2 in this study). According to the previous discussions in **Section 4.2**, the area of the interface for the rough and smooth surfaces should be determined as the effective area (A_{eff}) and are presented in **Figs. 22a** and **b**, respectively. The effective area of the interface (A_{eff}), the cross-section area of the yielded transverse rebars (A_s), and the ultimate prestressing levels (σ_u) are tabulated in **Table 7**.

Eventually, the predicted ultimate capacities using JSCE Specification, AASHTO, and *fib* MC2010 are listed in **Table 7** and are presented in **Fig. 23**. The calculation procedures for the rough (except for SL-Smooth) and smooth surfaces (SL-Smooth) were separated. This was because the values for constant in each design guideline were also separated based on the roughness degree of the interface (**Table 6**). The results demonstrated that all the selected design guidelines in both rough and smooth surfaces provided a good lower limit for the experimental ultimate capacities. From **Table 7**, JSCE Specification gave P_{EXP}/P_{CAL} that varied from 1.01 to 1.15 with a coefficient of variation (C.V.) of 4.3%. AASHTO specification provided P_{EXP}/P_{CAL} ratio that varied from 1.01 to 1.16 and C.V. of 4.7%. *fib* MC2010 gave P_{EXP}/P_{CAL} ratio that varied from 1.01 to 1.17 and C.V. of 5.0%.

Moreover, for the smooth surface, *fib* MC2010 gave the most accurate prediction compared to the other guidelines with P_{EXP}/P_{CAL} of 1.04 (**Table 7**). This was because *fib* MC2010 explicitly took into account the simultaneous action of bending resistance and axial resistance produced from the rebars crossing the interface (the dowel action), which was predominant in the smooth surface.

5. Conclusions

Based on the experimental results and FEM analyses of the widening prestressed concrete deck slabs crossed by steel bars and subjected to a concentrated load, the following conclusions can be drawn:

(1) The failure mode of the widening PC deck slabs supported on three sides and subjected to a concentrated load immediately adjacent to the interface is the shear failure of the interface between the old and new slabs. This failure mode is governed by the loss of confinement of rebars crossing the interface.

(2) The ultimate capacity of the PC deck slabs increases with the increase in the prestressing level and concrete strength of the new slab. However, it does not increase proportionally with the prestressing level and concrete strength.

(3) The variation in surface roughness of the interface does not show any remarkable influence on the ultimate capacity as long as the amount of prestress-

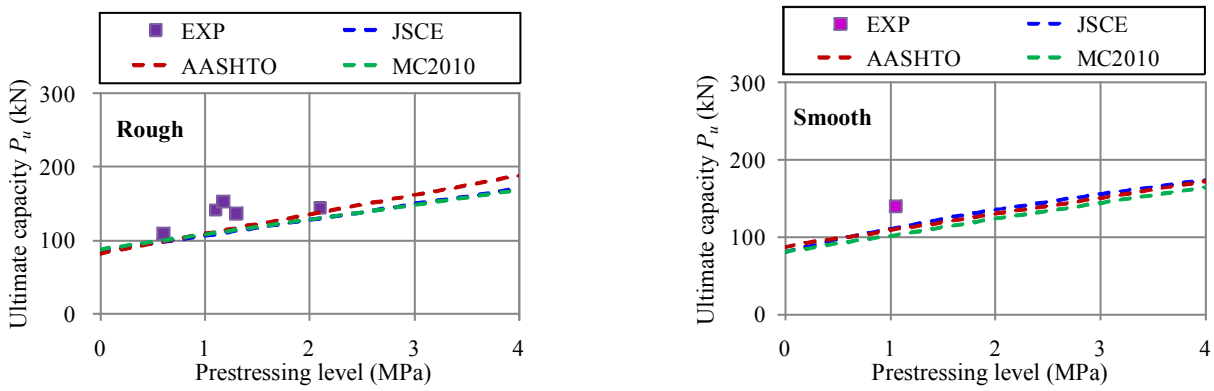

(a) Rough surface (except for SL-Smooth)

(b) Smooth surface (SL-Smooth)

Fig. 23 Accuracy of design guidelines.

ing force is sufficiently introduced to the interface. An obvious difference is only observed just before the failure, in which the shear slip occurs on the smooth surface.

(4) Experimental results and FEM analyses indicate that the prestressing levels of 1.0 MPa and 2.0 MPa can provide sufficient shear strength to the interface for transferring the shear stress to the adjacent deck slab.

(5) Coulomb friction model with and without cohesion coefficients is supposed to be appropriate to simulate the behavior of the interface between the old and new deck slabs crossed by steel bars and subjected to the prestressing force.

(6) The effective area of the interface for the widening PC deck slabs supported on three sides and subjected to a concentrated load is proposed in this study. It is required to compute the shear capacity of the interface using JSCE Specification, AASHTO, and fib Model Code 2010 instead of the total area of the interface as it was assumed in these guidelines. The calculated results indicate that all guidelines provide a good lower limit to predict the ultimate capacity of the interface.

References

AASHTO LRFD, (2007). "Bridge design specifications." *American Association of State Highway and Transportation Officials.*

Chigira, E., Niwa, J., Tanaka, Y. and Katagiri, M., (2007). "Study on punching shear resistance of the UFC panel." *Proceeding of the JCI*, 29(3), 1741-1746. (in Japanese)

Clement, T., Ramos, A., Ruiz, M. and Muttoni A., (2013). "Design for punching of prestressed concrete slabs." *Structural Concrete*, 12(2), 157-167.

Eder, M. A., Vollum, R. L., Elghazouli, A. Y. and Abdel-Fattah, T., (2010). "Modeling and experimental assessment of punching shear in flat slabs with shear-heads." *Engineering Structures*, 32, 3911-3924.

El-Gamal, S., El-Salakawy, E. and Benmokrane, B., (2007). "Influence of reinforcement on the behavior of concrete bridge deck slabs reinforced with FRP bars." *J. Compos. Constr.*, 11, 449-458.

Hamada, S., Yang, Q. and Mao, M., (2008). "Evaluation of punching shear strength of reinforced concrete slabs based on data base." *Journal of Advanced Concrete Technology*, 6(1), 205-214.

Haskett, M., Oehlers, D. J., Mohamed Ali, M. S. and Sharma, S. K., (2011). "Evaluating the shear-friction resistance across sliding planes in concrete." *Engineering Structures*, 33, 1357-1364.

Higashiyama, H. and Matsui, S., (1998). "Fatigue durability of longitudinally prestressed concrete slabs under running wheel." *JSCE J. Struct Mech Earthq Eng*, 605/I-45, 79-90. (in Japanese)

Hordijk, D. A., (1991). "*Local approach to fatigue of concrete*." Thesis (PhD). Delft University of Technology.

Hwang, H., Yoon, H., John, C. and Kim, B., (2010). "Punching and fatigue behavior of long-span prestressed concrete deck slabs." *Engineering Structures*, 32, 2861-2872.

International Federation for Structural Concrete, (2013). "Model code 2010."

Japan Road Association, (2012). "Design specification for highway bridges, Part III Concrete Bridges. (in Japanese)"

Japan Society of Civil Engineers, (2007). "Standard specification for design of concrete structures, structure performance verification."

Maekawa, K. and Qureshi, J., (1997). "Stress transfer across interfaces in reinforced concrete due to aggregate interlock and dowel action." *J. Materials, Conc. Struct., Pavements, JSCE*, 34(34), 159-172.

Mander, T. J., Mander, J. B. and Hite Head, M., (2011). "Modified yield line theory for full-depth precast concrete." *J. Bridge Eng.*, 16(1), 12-20.

Masui, T., Yamauchi, T., Morita, A., Sato, Y., Nishinaga, T., Tokumitsu, S., Yagi, Y., Yamada, M. and Yamaguchi, M., (25 April 2016). "*Widening PC floor version structure and widening construction method of established PC floor version*." Japanese Unexamined Patent Application Publication No. 2016-61045.

Muttoni, A. and Ruiz, M., (2012). "The levels-of-approximation approach in MC2010: Application to punching shear provisions." *Structural Concrete,* 13(1).

Niwa, J., Fakhruddin, Matsumoto, K., Sato, Y., Yamada, Y. and Yamauchi, T., (2016). "Experimental study on shear behavior of the interface between old and new deck slabs." *Engineering Structures*, 126, 278-291.

Rahal, K. N., Khaleefi, A. L. and Al-Sanee, A., (2016). "An experimental investigation of shear-transfer strength of normal and high strength self compacting concrete." *Engineering Structures*, 109, 16-25.

Randl, N., (2013). "Design recommendations for interface shear transfer in *fib* Model Code 2010." *Structural Concrete*, 14(3), 230-241.

Sivaleepunth, C., Niwa, J., Nguyen, D. H., Hasegawa, T. and Hamada, Y., (2009). "Shear carrying capacity of segmental prestressed concrete beam." *Journal of Materials, Concrete Structures and Pavements, JSCE*, 65(1), 63-75.

Thorenfeldt, E., Tomaszewicz, A. and Jensen, J. J., (1987). "Mechanical properties of high-strength concrete and application in design." *Symposium Proceeding of Utilization of High-Strength Concrete*, Norway.

Turmo, J., Ramos, G. and Aparicio, A. C., (2006). "FEM modeling of unbonded post-tensioned segmental beams with dry joints." *Engineering Structures*, 28, 1852-1863.